Pulse evolution without wave breaking in a strongly dissipative-dispersive laser system

Xueming Liu*

State Key Laboratory of Transient Optics and Photonics, Xi'an Institute of Optics and Precision Mechanics, Chinese Academy of Sciences, Xi'an 710119, China

(Received 8 March 2010; published 12 May 2010)

We report on pulse evolution without wave breaking in a strongly dissipative-dispersive laser system where pulses encounter significant amounts of positive and negative dispersions. In contrast to conventional soliton, dispersion-managed soliton, and self-similar pulse evolutions, a different type of pulse shaping in mode-locked lasers is theoretically investigated and experimentally observed. The pulses of this laser have very low frequency chirp and exhibit as the quasirectangle temporal and Gaussian spectral profiles, and the spectral width is almost independent of the pumping strength. The temporal and spectral widths fluctuate as low as ~3% of the relative fluctuation throughout the laser cavity. Both numerical and experimental results show that the pulses exist with energies much greater than can be tolerated in self-similar pulse shaping.

DOI: 10.1103/PhysRevA.81.053819 PACS number(s): 42.81.Dp, 42.55.Wd, 42.65.Tg, 42.65.Re

I. INTRODUCTION

Fiber-based sources attract extensive attention since they can produce high-energy ultrashort pulses, and nonlinear pulse evolution in fiber is a rich and fascinating subject [1–5]. Passively-mode-locked fiber lasers are able to easily generate self-starting short pulses [6–10]. Usually, pulses formed by the balance of (positive) nonlinear and (negative) dispersive phase shifts are limited to ~0.1 nJ of the pulse energy in standard fibers [11–13]. By adjusting the intracavity structure with the appropriate dispersion management, the passively-mode-locked fiber lasers underlie the order-of-magnitude increase in the pulse energy. Stretched-pulse fiber lasers, consisting of segments of anomalous and normal group-velocity dispersion (GVD), implement the concept of dispersion management and emit pulses with the pulse energy to reach the 1 nJ level [14,15]. Attempts to generate higher energies in stretched-pulse lasers constructed with single-mode fiber (SMF) always lead to multiple pulsing or other instabilities [12]. Instead of conventional solitons and dispersion-managed solitons, self-similar pulses can tolerate strong nonlinearity without wave breaking if they can evolve to fill available gain bandwidth. Because of the restricted gain bandwidth (e.g., ~30 nm for erbium-doped fiber), the self-similar pulse encounters a limitation to its spectral bandwidth, and thus self-similar propagation of intense pulses is disrupted [16]. Self-similar pulses allow the pulse energy to reach the 10-nJ level [12,17,18]. Although the aforementioned techniques can effectively decrease the effects of nonlinearity through dispersion management, they do not eliminate the limitation of nonlinear effects.

All-normal-dispersion lasers can enhance the self-amplitude modulation through chirped-pulse spectral filtering and stabilize high-energy coherent pulses without dispersion management. Pulse shaping based on spectral filtering feature highly chirped pulses in the laser cavity. All-normal-dispersion lasers generate the highly chirped pulses with pulse energy of >20 nJ [19]. As the pulse energy increases, the spectral shaping, owing to the finite gain bandwidth of the medium, plays a key role. The accumulation of excessive nonlinear phase shift or excessive pulse chirp thus causes the pulse to break up [12,20].

In order to substantially increase the pulse energy, direct management of nonlinearity of the laser cavity has been used to construct lasers. High-energy lasers with scaling at constant nonlinear phase shift can be accomplished using large-mode-area fibers [21–23]. However, this solution complicates the design of the laser cavity and eliminates the alignment-free waveguide format, due to the use of free-space components.

Wave breaking is the fundamental limit to pulse energy. Fortunately, highly chirped pulses can reach unprecedented energies and peak powers and avoid wave breaking despite the accumulation of large nonlinear phase shifts. Anderson *et al.* showed that wave breaking is avoided when a pulse acquires a monotonic frequency sweep or chirp as it propagates [24]. They proved that when the GVD is normal, high-intensity solutions without wave breaking exist for the nonlinear Schrödinger equation. Tamura *et al.* found that the evolution to a parabolic shape reduced wave breaking in a short-pulse fiber amplifier [25]. Jones *et al.* showed that lasers operated close to the self-similar regime exhibited operation without wave breaking with peak power five times that of a dispersion-managed soliton laser [26]. Ilday *et al.* found that stable self-similar pulses existed with energies much greater than could be tolerated in solitonlike pulse shaping [16]. However, both dispersion-managed soliton lasers and self-similar parabolic-pulse lasers do not completely eliminate the limitations of wave breaking.

In this article, a different type of pulse shaping in mode-locked lasers is theoretically investigated and experimentally observed. Pulse evolution without wave breaking in a strongly dissipative-dispersive laser system is observed numerically and experimentally. The pulse evolution in our laser is qualitatively distinct from the well-known conventional soliton, dispersion-managed soliton, and self-similar pulse evolutions. The experimental observations confirm the theoretical predictions.

II. EXPERIMENTAL SETUP AND MECHANISMS

The proposed fiber laser oscillator is shown schematically in Fig. 1. The laser cavity consists of a polarization-sensitive

*liuxm@opt.ac.cn

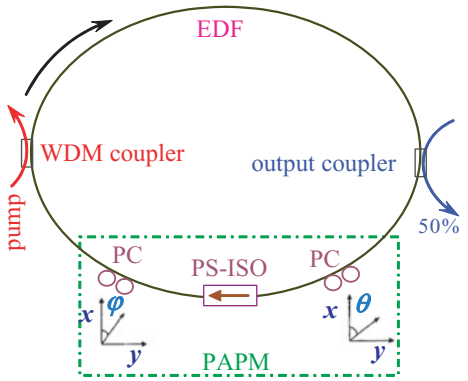

FIG. 1. (Color online) Schematic diagram of laser cavity through the PAPM element.

isolator (PS-ISO), two sets of polarization controllers (PCs), a fused coupler with 50% output, a wavelength-division multiplexing (WDM) coupler, and a piece of erbium-doped fiber (EDF). A PS-ISO combined with two PCs forms a polarization additive pulse-mode-locking (PAPM) element. The total length of laser cavity is about 25.5 m, including an EDF of about 18 m and an SMF of about 7.5 m. The EDF and SMF have dispersion parameters of about 55×10^{-3} and -22×10^{-3} ps^2/m at 1550 nm, respectively. The gain medium of EDF has a gain bandwidth of 30 nm, and its normalized spectral profile can be approximated by $g_{\mathrm{nor}}(\omega) = 1/[1 + (\omega/\Delta\omega)^6]$, where ω and $\Delta\omega$ are the frequency detuning and the EDF bandwidth, respectively.

The EDF and SMF provide large positive and negative dispersions of about 1 ps^2 and -0.17 ps^2 to a laser system, respectively. A laser with large net normal GVD would presumably have to exploit dissipative processes in the mode-locked pulse shaping, which has major contributions from gain and loss processes in addition to the phase modulations [12,27]. So the pulses in the proposed laser system have to encounter significant amounts of dispersion (positive and negative) and suffer large loss (and gain). The strongly dissipative and dispersive mechanisms will influence the pulse formation.

III. THEORETICAL MODELING

Usually, the lightwave propagation in the weakly birefringent fibers is modeled by the two coupled equations that involve a vector electric field. In this work, the fiber length of laser cavity, L, is much larger than its beat length L_B (here $L \approx 25.5$ m and $L_B \approx 1$ m). The physical terms involved in L_B are considered to be negligible. To describe the light propagation, we used coupled complex nonlinear Schrödinger equations of the form [28,29]

$$\frac{\partial u}{\partial z} = -\frac{\alpha}{2}u - \delta\frac{\partial u}{\partial T} - i\frac{\beta_2}{2}\frac{\partial^2 u}{\partial T^2} + i\gamma\left(|u|^2 + \frac{2}{3}|v|^2\right)u + \frac{g}{2}u + \frac{g}{2\Omega_g^2}\frac{\partial^2 u}{\partial T^2},$$
$$\frac{\partial v}{\partial z} = -\frac{\alpha}{2}v + \delta\frac{\partial v}{\partial T} - i\frac{\beta_2}{2}\frac{\partial^2 v}{\partial T^2} + i\gamma\left(|v|^2 + \frac{2}{3}|u|^2\right)v + \frac{g}{2}v + \frac{g}{2\Omega_g^2}\frac{\partial^2 v}{\partial T^2}. \quad (1)$$

Here, u and v denote the envelopes of the optical pulses along the two orthogonal polarization axes of the fiber; α is the loss coefficient of fiber. The modal birefringence of fiber is given by $\Delta\beta = \beta_{0x} - \beta_{0y}$, where β_{0j} is the propagation constant ($j = x, y$). β_{1x} and β_{1y} are the group velocities of the two polarization components, β_2 represents the fiber dispersion, γ refers to the cubic refractive nonlinearity of the medium, Ω_g is the bandwidth of the laser gain, $\delta = (\beta_{1x} - \beta_{1y})/2$ is the group-velocity difference between the two polarization modes, and $T = t - (\beta_{1x} + \beta_{1y})z/2$. The variables t and z indicate the pulse local time and the propagation distance, respectively, and g is the net gain, which is nonzero only for the amplifier fiber. It describes the gain function of EDF and is expressed by [29]

$$g = g_0 \exp(-E_p/E_s). \quad (2)$$

Here, g_0 is the small-signal gain with a bandwidth of 30 nm. E_s is the gain saturation energy, which is dependent on pump power [30,31]. The pulse energy E_p is given by

$$E_p = \int_{-T_R/2}^{T_R/2} (|u|^2 + |v|^2) d\zeta, \quad (3)$$

where T_R is the cavity round-trip time.

The light transmission through fibers can be simulated by solving Eqs. (1)–(3) and by using spectral filtering [28]. When the light propagates through the PAPM element, the intensity transmission of light, T, is expressed as

$$T = \sin^2(\theta)\sin^2(\varphi) + \cos^2(\theta)\cos^2(\varphi) + 0.5\sin(2\theta)\sin(2\varphi)\cos(\phi_1 + \phi_2), \quad (4)$$

where ϕ_1 is the phase delay caused by the polarization controllers and ϕ_2 is the phase delay resulting from the fiber, including both the linear phase delay and the nonlinear phase delay. The polarizer and analyzer have an orientation of angles θ and φ with respect to the fast axis of the fiber, respectively (Fig. 1). Obviously, two coupled-mode equations [i.e., Eq. (1)] describing the lightwave propagation in the weakly birefringent fibers involve a vector electric field. Komarov *et al.* had proposed a simplified model where the two-component system reduces to a single Ginzburg-Landau equation [32].

IV. SIMULATION RESULTS

The numerical model is solved with a predictor-corrector split-step Fourier method [33]. The simulation started from an arbitrary signal and converged into a stable solution with appropriate parameters after a finite number of traversals of the cavity. Numerical simulations show that, for fixed parameters, exactly the same stable solutions are reached from distinct initial noise fields. By appropriately setting the polarization of polarizer and analyzer and the linear cavity phase-delay bias of the cavity, self-started mode locking can be achieved in a multipulse operation or single-pulse operation without wave breaking. We use the following parameters for our simulations for possibly matching the experimental conditions: $\alpha = 0.2$ dB/km, $g_0 = 2$ m^{-1}, $\gamma = 4.5$ W^{-1} km^{-1} for EDF and 1.3 W^{-1} km^{-1} for SMF, $\Omega_g = 30$ nm, $\beta_2 = 55 \times 10^{-3}$ ps^2/m for EDF and -22×10^{-3} ps^2/m for SMF, and the net cavity GVD $\beta_{\mathrm{net}} \approx 0.83$ ps^2.

Since the saturation energy E_s is proportional to the pumping strength [31], increasing E_s corresponds to increasing the pump power in the experiments. Numerical results show that the stable solutions of mode-locking lasers are very sensitive to the angles θ and φ and the phase delay ϕ_1. For instance, when $\theta = \pi/3.8$, $\varphi = \pi/4.5$, and $\phi_1 = 0.3 + \pi/2$, the pulse number over a cavity round-trip time is generated one by one with the increase of the pumping parameter E_s. On the other hand, the typical single-pulse solution without wave breaking can be obtained with $\theta = \pi/4$, $\varphi = \pi/10$, and $\phi_1 = 0.25 + \pi/2$, as shown in Fig. 2; θ, φ, and ϕ_1 in experiments are determined by the state of two PCs.

Figure 2(a) shows that the pulse width broadens gradually as a function of the pumping strength E_s, whereas the peak power increases slowly with E_s. For increasing E_s, both pulse width and pulse energy increase with an approximately linear evolution, as shown in Fig. 2(c). For instance, the pulse width is enhanced by a factor of 8 when E_s is increased from 2.5 to 25 nJ [Fig. 2(c)], whereas the peak power of pulses is a factor of 1.3 higher in this case. Therefore, the nonlinear phase shift ϕ of pulses increases slowly (ϕ is proportional to the peak power of pulses), although the pulse energy is enhanced greatly.

Figure 2(b) shows that, for increasing E_s, the spectral width almost keeps a constant, although the spectral peak increases remarkably. The detailed evolution is demonstrated in Fig. 2(d). It appears that the spectral width decreases in a lower E_s (e.g., $E_s < 10$ nJ) and then approaches a constant. Surprisingly, the optical spectrum of our laser approximately is the Gaussian profile, instead of the quasirectangular profile that is the typical spectrum of net-normal-GVD mode-locked fiber lasers. Moreover, the spectral width of our laser is independent of the pumping strength E_s, so that our laser intrinsically overcomes the limit of bandwidth of gain fibers and has the capacity of generating ultra-high-energy pulses. It is found from Fig. 2 that the time-bandwidth product increases almost linearly for $E_s > 5$ nJ. The theoretical results show that the chirp of pulses remains constant when E_s is more than 10 nJ.

Obviously, the evolution of pulse properties of our laser is qualitatively distinct from that of self-similar lasers. Because the spectral width increases substantially in self-similar amplification, the self-similar lasers have to be subsequently amplified with a short segment of gain fiber in the presence of minimal dispersion and nonlinearity. As a result, the pulse energy in the self-similar lasers is limited by a shorter gain fiber (e.g., 23-cm-long gain fiber [16]). However, the gain fiber here is as long as 18 m because the spectral width of our laser is almost independent of the amplification of gain fiber.

Figure 3 shows the temporal power profile and instantaneous frequency of the pulses at a typical $E_s = 25$ nJ. The corresponding autocorrelation trace is shown in inset. One can observe from Fig. 3 that pulses have approximately rectangular temporal profiles, different from the parabolic, Gaussian, and hyperbolic-secant temporal profiles shown in self-similar, dispersion-managed soliton, and conventional soliton lasers, respectively. The pulse chirp is nearly linear across the central region of pulse, whereas it is nonlinear at the edges of pulse. The linear part has very low chirp, varying from -1.5 to 1.5 THz, which is over twenty times less than the pulse chirp of self-similar lasers [12,16]. Since

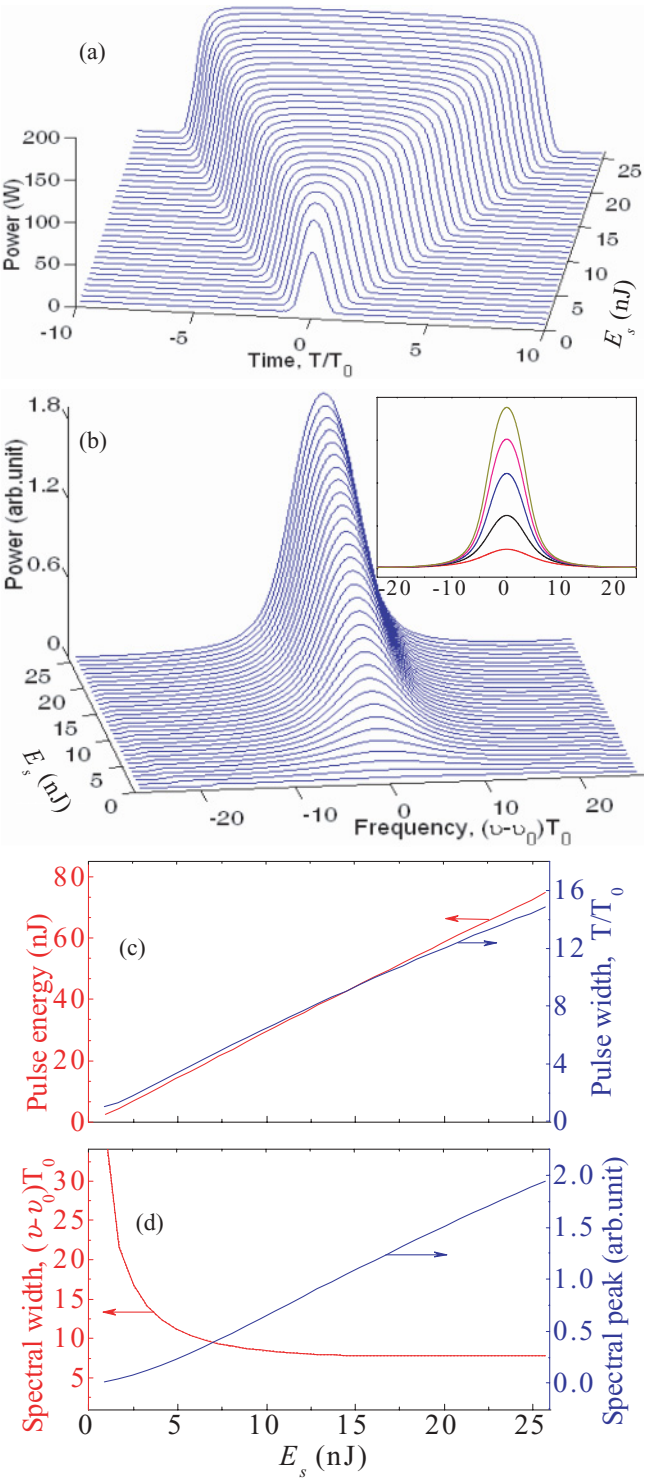

FIG. 2. (Color online) Results of numerical simulations. (a) Pulse evolution as a function of pumping strength E_s. T_0 is the pulse duration at $E_s = 1$ nJ. (b) Power evolution with E_s in the spectral domain. Some typical power spectra are shown in inset: $E_s = 5$, 10, 15, 20, and 25 nJ from bottom to top, respectively. (c) Pulse energy and pulse width versus E_s. (d) Spectral width and peak versus E_s.

different frequency components of a pulse travel at different speeds along the laser system [34], very low frequency chirp means that the frequency components of the pulse travel at approximately the same speed. The nonlinear chirp at the

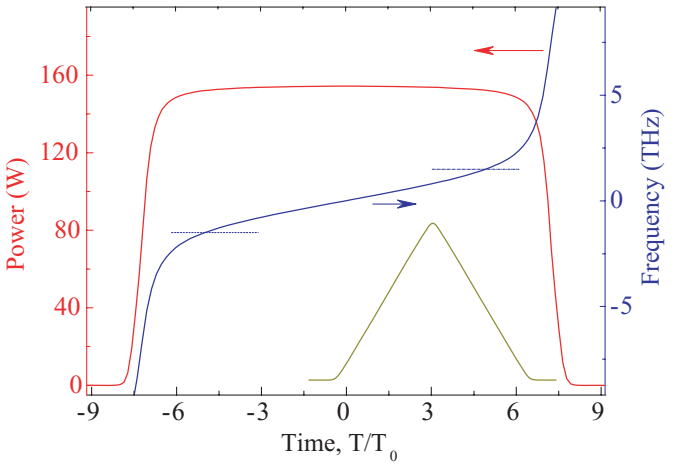

FIG. 3. (Color online) Numerical simulations of temporal power profile (left) and instantaneous frequency (right) of the pulses at $E_s = 25$ nJ. Inset: the corresponding autocorrelation trace.

edge of the pulse can resist the influence of larger dispersion that causes the linear chirp to pulse. Therefore, very low frequency chirp on the central region of the pulse, together with the nonlinear chirp at the edge of the pulse, maintain the pulse in operation without wave breaking in a high-energy regime.

Recently, the dissipative soliton resonance (DSR) technique is used to achieve high-energy pulses [35]. When the parameters of the laser are closer to the resonance point, high-energy pulses appear at this resonance and the shape of the pulses is closer to being rectangular. Although the rectangular pulses with Gaussian spectra exhibited in the DSR are similar to our results, their chirps have some difference. The chirps of pulses in DSR are linear across the whole pulse, whereas the chirps of pulses here are nonlinear at the edges of pulses (Fig. 3). Of course, the pulses in this report can be an example of approximate DSR.

The pulse characteristics in the intracavity position are illustrated in Fig. 4. Figures 4(a) to 4(c) show the intracavity pulse evolutions in the temporal domain, spectral domain, and instantaneous frequency over a cavity round trip at $E_s =$ 25 nJ, respectively. One can see from Figs. 4(a) and 4(b) that the relative fluctuations of the temporal and spectral widths of pulses during the intracavity propagation are as low as ~3%, very different from the pulse behavior in the multipulse operation regime where the temporal and spectral breathing ratios are more than two [36]. It is very surprising that the chirp of pulses hardly fluctuates throughout the laser cavity, as shown in Fig. 4(c). The pulse peak and its spectral peak rapidly increase in the beginning of the EDF and then slightly vary in the remaining EDF part. It is found from Figs. 4(a) and 4(b) that the pulses with quasirectangle temporal and Gaussian spectral profiles exist throughout the laser cavity.

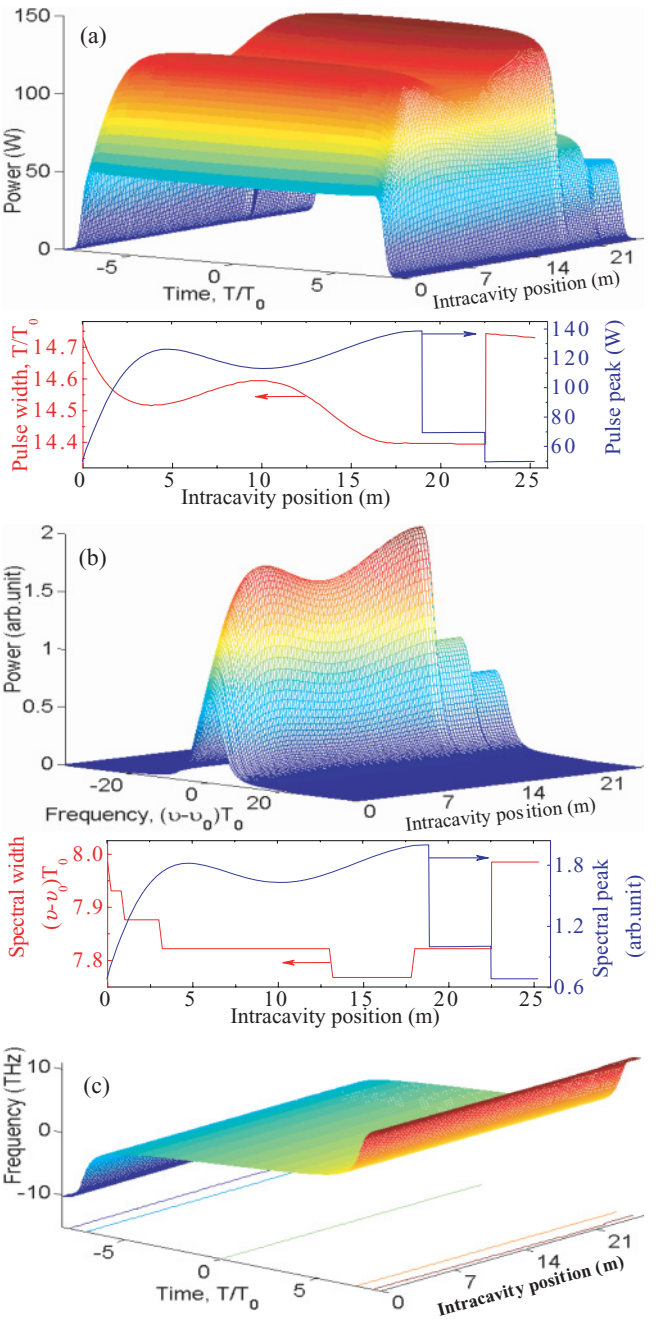

FIG. 4. (Color online) Intracavity pulse evolutions in (a) the temporal domain (top plot: three-dimension evolutions; bottom plot: two-dimension evolutions for pulse energy and width), (b) the spectral domain (top plot: three-dimension evolutions; bottom plot: two-dimension evolutions for spectral width and peak), and (c) the instantaneous frequency at $E_s = 25$ nJ throughout the laser cavity. Intracavity position: EDF from 0 to 18 m, output coupler at 19 m, and PAPM at 22.5 m.

V. EXPERIMENTS AND COMPARISONS

With appropriate orientation and pressure settings on the two PCs, the self-started mode locking of the laser is achieved at the threshold pump power $P \approx 80$ mW. The laser operation is simultaneously monitored using an autocorrelator, optical spectrum analyzer (OSA), and radio-frequency (rf) spectrum analyzer. Figures 5(a)–5(d) demonstrate the optical spectrum of the pulses, the autocorrelation trace, and the rf spectrum, respectively. Figure 5(a) shows some typical output spectra ($P = 100, 200, 300, 400$, and 500 mW), centered at ~1567 nm, with full width at half maximum (FWHM) of 11~14 nm.

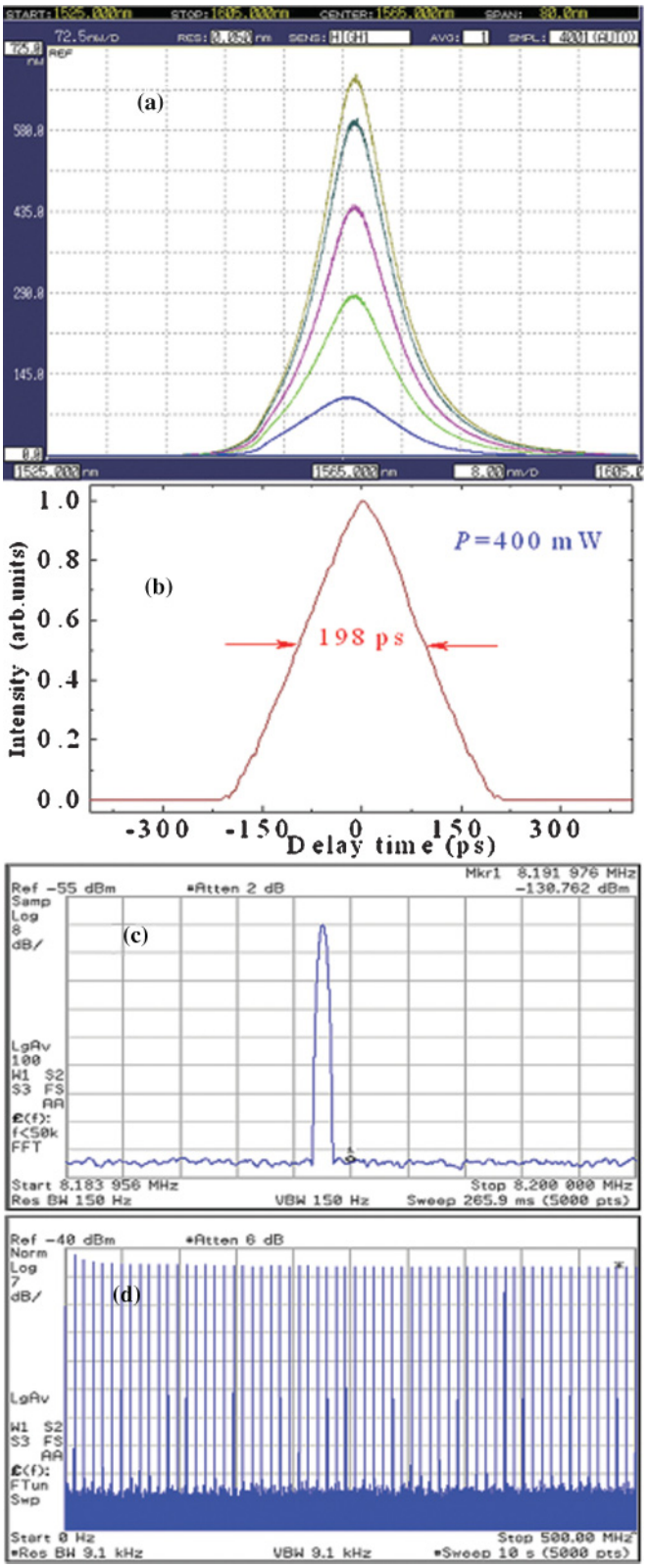

FIG. 5. (Color online) Results of experimental observations: (a) Output optical spectrum. Pump power $P = 100, 200, 300, 400$, and 500 mW from bottom to top, respectively. (b) Autocorrelation trace for $P = 400$ mW. (c) Fundamental rf spectrum of the laser output. (d) Wideband rf spectrum up to 500 MHz.

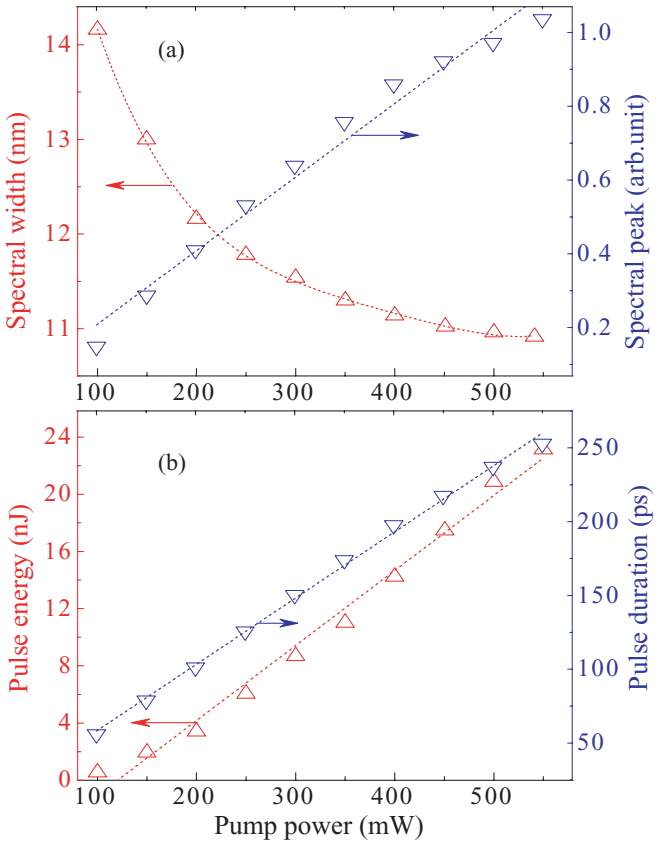

FIG. 6. (Color online) Experimental results of (a) spectral width and peak vs pump power and (b) intracavity pulse energy and duration vs pump power.

One can see from Figs. 2(b) and 5(a) that the experimental results are in good agreement with the theoretical predictions that the optical spectrum of pulses is similar to the Gaussian profile. Both experimental and numerical results illustrate that the spectral behaviors of this laser are different from the typical spectrum characteristics of all- or net-normal-dispersion mode-locked fiber lasers where there are steep spectral edges.

The experimental observations show that the autocorrelation trace of the pulse has a quasitriangular profile. An typical example for $P \approx 400$ mW is illustrated in Fig. 5(b), and the experimental results confirm the theoretical predictions (inset of Fig. 3). Figure 5(c) shows a measurement made at a resolution bandwidth of 150 Hz. The fundamental peak located at the cavity repetition rate of 8.19 MHz has a signal-to-noise ratio of ~70 dB. Figure 5(d) shows the wideband rf spectrum up to 500 MHz. The rf spectrum confirms the stable mode locking and absence of sidebands and harmonic frequencies to 60 dB below the fundamental frequency.

The stable mode locking with the single-pulse operation is always maintained in the laser as the pump power P is gradually increased. The intracavity pulse energy and duration increase almost linearly with P. The experimental results are shown in Fig. 6(b) in detail. The experimental observations are in good agreement with the theoretical predictions [3,37]

and confirm the existence of the dissipative-soliton-resonance phenomenon. Figure 6(a) shows the evolutions of spectral width and peak as functions of P. It appears that the spectral peak increases approximately linearly with P. However, the spectral width decreases monotonically for lower pump power (e.g., $P < 400$ mW), and successively it approximately approaches constant for higher P.

VI. CONCLUSIONS

Pulse evolution without wave breaking in a large net-normal-GVD mode-locked fiber laser is investigated numerically and experimentally. Pulses in such lasers encounter significant amounts of dispersion (positive and negative) and are influenced by the strongly dissipative and dispersive mechanisms. A different type of pulse shaping in mode-locked lasers is theoretically investigated and experimentally observed, which is qualitatively distinct from previously identified mode-locking techniques. The pulses have the quasirectangular temporal profile and the Gaussian spectral profile, different from the pulses shown in self-similar, dissipative-soliton, and conventional-soliton lasers, respectively. The pulse of our laser has very low frequency chirp, and its spectral width is almost independent of the pumping strength, so the single-pulse operation without wave breaking can be maintained in the strongly high-energy regime. The chirp of pulses hardly fluctuates throughout the laser cavity, and the pulses have the relative fluctuations of the temporal and spectral widths as low as ~3%. Numerical and experimental results show that pulse energies one to two orders of magnitude larger than those of existing lasers should be possible.

ACKNOWLEDGMENTS

This work was supported by the National Natural Science Foundation of China under Grant Nos. 10874239 and 10604066. The author especially thanks Dong Mao, Leiran Wang, and Xiaohui Li for help with the experiments.

[1] V. I. Kruglov, D. Méchin, and J. D. Harvey, Phys. Rev. A **81**, 023815 (2010).
[2] A. Komarov and F. Sanchez, Phys. Rev. E **77**, 066201 (2008).
[3] W. Chang, J. M. Soto-Crespo, A. Ankiewicz, and N. Akhmediev, Phys. Rev. A **79**, 033840 (2009).
[4] V. Roy, M. Olivier, F. Babin, and M. Piché, Phys. Rev. Lett. **94**, 203903 (2005).
[5] J. N. Kutz, Phys. Rev. A **78**, 013845 (2008).
[6] A. Haboucha, H. Leblond, M. Salhi, A. Komarov, and F. Sanchez, Phys. Rev. A **78**, 043806 (2008).
[7] M. Salhi, A. Haboucha, H. Leblond, and F. Sanchez, Phys. Rev. A **77**, 033828 (2008).
[8] A. Zavyalov, R. Iliew, O. Egorov, and F. Lederer, Phys. Rev. A **79**, 053841 (2009).
[9] W. H. Renninger, A. Chong, and F. W. Wise, Phys. Rev. A **77**, 023814 (2008).
[10] R. Weill, B. Vodonos, A. Gordon, O. Gat, and B. Fischer, Phys. Rev. E **76**, 031112 (2007).
[11] L. Nelson, D. Jones, K. Tamura, H. Haus, and E. Ippen, Appl. Phys. B **65**, 277 (1997).
[12] F. Wise, A. Chong, and W. Renninger, Laser Photon. Rev. **2**, 58 (2008).
[13] X. Wu, D. Y. Tang, L. M. Zhao, and H. Zhang, Phys. Rev. A **80**, 013804 (2009).
[14] K. Tamura, E. P. Ippen, H. A. Haus, and L. E. Nelson, Opt. Lett. **18**, 1080 (1993).
[15] N. Smith, N. Doran, W. Forysiak, and F. Knox, J. Lightwave Technol. **15**, 1808 (1997).
[16] F. O. Ilday, J. R. Buckley, W. G. Clark, and F. W. Wise, Phys. Rev. Lett. **92**, 213902 (2004).
[17] T. Lei, F. Lu, C. Tu, Y. Deng, and E. Li, Opt. Express **17**, 585 (2009).
[18] J. Buckley, F. Wise, F. Ilday, and T. Sosnowski, Opt. Lett. **30**, 1888 (2005).
[19] A. Chong, W. Renninger, and F. Wise, Opt. Lett. **32**, 2408 (2007).
[20] X. Liu, L. Wang, X. Li, H. Sun, A. Lin, K. Lu, Y. Wang, and W. Zhao, Opt. Express **17**, 8506 (2009); X. Liu, *ibid.* **17**, 9549 (2009).
[21] C. Lecaplain, B. Ortaç, and A. Hideur, Opt. Lett. **34**, 3731 (2009).
[22] B. Ortaç, O. Schmidt, T. Schreiber, J. Limpert, A. Tünnermann, and A. Hideur, Opt. Express **15**, 10725 (2007).
[23] Y. Song, M. Hu, C. Wang, Z. Tian, Q. Xing, L. Chai, and C. Wang, IEEE Photon. Technol. Lett. **20**, 1088 (2008).
[24] D. Anderson, M. Desaix, M. Karlsson, M. Lisak, and M. L. Quiroga-Teixeiro, J. Opt. Soc. Am. B **10**, 1185 (1993).
[25] K. Tamura and M. Nakazawa, Opt. Lett. **21**, 68 (1996).
[26] D. Jones, H. A. Haus, L. Nelson, and E. Ippen, IEICE Trans. Electron. **E81C**, 180 (1998).
[27] N. Akhmediev and A. Ankiewicz, eds., *Dissipative Solitons* (Springer, Berlin, 2005).
[28] X. Liu, Phys. Rev. A **81**, 023811 (2010).
[29] G. Agrawal, IEEE Photon. Technol. Lett. **2**, 875 (1990).
[30] A. Cabasse, B. Ortaç, G. Martel, A. Hideur, and J. Limpert, Opt. Express **16**, 19322 (2008).
[31] G. Martel, C. Chédot, V. Réglier, A. Hideur, B. Ortaç, and P. Grelu, Opt. Lett. **32**, 343 (2007).
[32] A. Komarov, H. Leblond, and F. Sanchez, Phys. Rev. E **72**, 025604(R) (2005).
[33] X. Liu and B. Lee, IEEE Photon. Technol. Lett. **15**, 1549 (2003).
[34] G. P. Agrawal, *Nonlinear Fiber Optics*, 4th ed. (Academic Press, Boston, 2007).
[35] W. Chang, A. Ankiewicz, J. M. Soto-Crespo, and N. Akhmediev, J. Opt. Soc. Am. B **25**, 1972 (2008).
[36] X. Liu, Opt. Express **17**, 22401 (2009).
[37] A. Chong, W. H. Renninger, and F. W. Wise, J. Opt. Soc. Am. B **25**, 140 (2008).